Agostic-Type B−H···Pb Interactions Stabilize a Dialkylplumbylene. Structure of and Bonding in [{nPr$_2$P(BH$_3$)}(Me$_3$Si)C(CH$_2$)]$_2$Pb

Keith Izod,* William McFarlane, Corinne Wills, William Clegg, and Ross W. Harrington

Main Group Chemistry Laboratory and Crystallography Laboratory, School of Chemistry, Bedson Building, University of Newcastle, Newcastle upon Tyne, NE1 7RU, U.K.

Received June 27, 2008

The reaction between Cp$_2$Pb and 1 equiv of [[{nPr$_2$P(BH$_3$)}(Me$_3$Si)C(CH$_2$)]Li(THF)$_2$]$_2$ in toluene affords the dialkylplumbylene [{nPr$_2$P(BH$_3$)}(Me$_3$Si)C(CH$_2$)]$_2$Pb (**10**) in excellent yield; compound **10** may readily be separated into its two diastereomeric forms by a simple crystallization procedure. X-ray crystallography shows that *rac*- and *meso*-**10** crystallize as discrete dialkylplumbylenes in which there are either two (*rac*-**10**) or one (*meso*-**10**) short agostic-type B−H···Pb contacts; for *meso*-**10** there is a secondary, weak B−H···Pb contact, which affords this diastereomer a further, weak stabilization. Multielement and variable-temperature NMR studies indicate that, while *rac*-**10** is essentially static in solution, *meso*-**10** undergoes dynamic exchange between the free and bound BH$_3$ groups. Unusually, the methylene backbone protons in both diastereomers (at low temperature for *meso*-**10**) lie within the range 2.5−6.5 ppm, possibly due to the close proximity of the 6s lone pair on the lead center. DFT studies indicate that there is significant delocalization of B−H σ-bonding electron density into the vacant lead 6p orbital, furnishing an overall stabilization of 40.6 and 30.3 kcal mol^{-1} for *rac*- and *meso*-**10**, respectively.

Introduction

The synthesis of stable heavier group 14 carbene analogues (diorganotetrylenes) remains a fascinating and challenging area of contemporary main group chemistry. Over the last three decades enormous strides have been made in the synthesis of heteroatom-stabilized tetrylenes, analogues of the Arduengo-type N-heterocyclic carbenes and their acyclic counterparts, in which the electron deficiency of the tetrel center is mitigated by p$_\pi$−p$_\pi$ interactions between the lone pairs on the heteroatoms and the vacant p orbital on the tetrel center.[1−4] By contrast, the chemistry of hydrocarbyl-substituted diorganotetrylenes, in which such stabilizing interactions are absent, has been much less well explored, although, in recent years, several examples of sterically hindered diaryltetrylenes Ar$_2$E (E = Si, Ge, Sn, Pb) have been reported;[5] there have been few reports of the corresponding dialkyltetrylenes (R$_3$C)$_2$E. Until recently, crystallographically characterized dialkyltetrylenes were limited to the cyclic species reported by Kira and co-workers (**1**−**3**),[6−8] the acyclic dialkylgermylene reported by Jutzi and co-workers (**4**),[9] and the highly sterically hindered tin and lead metallacycles reported by Eaborn, Smith, and co-workers (**5**, **6**) (Chart 1);[10,11] of these compounds, only one is a dialkylplumbylene. In addition to the foregoing, a range of sterically hindered

* Corresponding author. E-mail: k.j.izod@ncl.ac.uk.

(1) For recent reviews of heavier tetrylene chemistry see:(a) Barrau, J.; Rima, G. *Coord. Chem. Rev.* **1998**, *178*−*180*, 593. (b) Tokitoh, N.; Okazaki, R. *Coord. Chem. Rev.* **2000**, *210*, 251. (c) Kira, M. *J. Organomet. Chem.* **2004**, *689*, 4475. (d) Weidenbruch, M. *Eur. J. Inorg. Chem.* **1999**, 373. (e) Klinkhammer, K. W. In *Chemistry of Organic Germanium, Tin and Lead Compounds*; Rappoport, Z., Ed.; Wiley: New York, 2002; Vol. 2, pp 283−357. (f) Veith, M. *Angew. Chem., Int. Ed. Engl.* **1987**, *26*, 1.

(2) For leading references to diamidogermylenes, -stannylenes, and -plumbylenes see:(a) Fjeldberg, T.; Hope, H.; Lappert, M. F.; Power, P. P.; Thorne, A. J. *J. Chem. Soc., Chem. Commun.* **1983**, 639. (b) Olmstead, M. M.; Power, P. P. *Inorg. Chem.* **1984**, *23*, 413. (c) Tang, Y.; Felix, A. M.; Zakharov, L. N.; Rheingold, A. L.; Kemp, R. A. *Inorg. Chem.* **2004**, *43*, 7239. (d) Avent, A. G.; Drost, C.; Gehrus, B.; Hitchcock, P. B.; Lappert, M. F. *Z. Anorg. Allg. Chem.* **2004**, *630*, 2090. (e) Gans-Eichler, T.; Gudat, D.; Nieger, M. *Angew. Chem., Int. Ed.* **2002**, *41*, 1888. (f) Chorley, R. W.; Hitchcock, P. B.; Lappert, M. F.; Leung, W.-P.; Power, P. P.; Olmstead, M. M. *Inorg. Chim. Acta* **1992**, *198*, 203. (g) Braunschweig, H.; Hitchcock, P. B.; Lappert, M. F.; Pierssens, L. J.-M. *Angew. Chem., Int. Ed. Engl.* **1994**, *33*, 1156. (h) Lappert, M. F.; Slade, M. J.; Atwood, J. L.; Zaworotko, M. J. *J. Chem. Soc., Chem. Commun.* **1980**, 621. (i) Bazinet, P.; Yap, G. P. A.; Richeson, D. S. *J. Am. Chem. Soc.* **2001**, *123*, 11162.

(3) For a comprehensive review of the chemistry of N-heterocyclic germylenes see:Kühl, O. *Coord. Chem. Rev.* **2004**, *248*, 411.

(4) For recent reviews of N-heterocyclic silylenes see:(a) Hill, N. J.; West, R. *J. Organomet. Chem.* **2004**, *689*, 4165. (b) Gehrhus, B.; Lappert, M. F. *J. Organomet. Chem.* **2001**, *617*, 209.

(5) (a) Yang, X.-J.; Wang, Y.; Wei, P.; Quillan, B.; Robinson, G. H. *Chem. Commun.* **2006**, 403. (b) Phillips, A. D.; Hino, S.; Power, P. P. *J. Am. Chem. Soc.* **2003**, *125*, 7520. (c) Pu, L.; Olmstead, M. M.; Power, P. P.; Schiemenz, B. *Organometallics* **1998**, *17*, 5602. (d) Stürmann, M.; Weidenbruch, M.; Klinkhammer, K. W.; Lissner, F.; Marsmann, H. *Organometallics* **1998**, *17*, 4425. (e) Lay, U.; Pritzkow, H.; Grützmacher, H. *Chem. Commun.* **1992**, 260. (f) Simons, R. S.; Pu, L.; Olmstead, M. M.; Power, P. P. *Organometallics* **1997**, *16*, 1920. (g) Grützmacher, H.; Pritzkow, H.; Edelmann, F. T. *Organometallics* **1991**, *10*, 23. (h) Brooker, S.; Buijink, J.-K.; Edelmann, F. T. *Organometallics* **1991**, *10*, 25. (i) Tajima, T.; Takeda, N.; Sasamori, T.; Tokitoh, N. *Organometallics* **2006**, *25*, 3552. (j) Spikes, G. H.; Peng, Y.; Fettinger, J. C.; Power, P. P. *Z. Anorg. Allg. Chem.* **2006**, *632*, 1005. (k) Wegner, G. L.; Berger, R. J. F.; Schier, A.; Schmidbaur, H. *Organometallics* **2001**, *20*, 418. (l) Weidenbruch, M.; Schlaefke, J.; Schafer, A.; Peters, K.; von Schnering, H. G.; Marsmann, H. *Angew. Chem., Int. Ed. Engl.* **1994**, *33*, 1846. (m) Braunschweig, H.; Drost, C.; Hitchcock, P. B.; Lappert, M. F.; Pierssens, L. J.-M. *Angew. Chem., Int. Ed. Engl.* **1997**, *36*, 261. (n) Bender, J. E.; Banaszak Holl, M. K.; Kampf, J. W. *Organometallics* **1997**, *16*, 2743. (o) Kano, N.; Shibita, K.; Tokitoh, N.; Okazaki, R. *Organometallics* **1999**, *18*, 2999. (p) Jutzi, P.; Schmidt, H.; Neumann, B.; Stammler, H.-G. *Organometallics* **1996**, *15*, 741. (q) Pu, L.; Twamley, B.; Power, P. P. *Organometallics* **2000**, *19*, 2874.

(6) Kira, M.; Yauchibara, R.; Hirano, R.; Kabuto, C.; Sakurai, H. *J. Am. Chem. Soc.* **1991**, *113*, 7785.

(7) Kira, M.; Ishida, S.; Iwamoto, T.; Kabuto, C. *J. Am. Chem. Soc.* **1999**, *121*, 9722.

(8) Kira, M.; Ishida, S.; Iwamoto, T.; Ichinohe, M.; Kabuto, C.; Ignatovich, L.; Sakurai, H. *Chem. Lett.* **1999**, 263.

(9) Jutzi, P.; Becker, A.; Stammler, H. G.; Neumann, B. *Organometallics* **1991**, *10*, 1647.

(10) Eaborn, C.; Hill, M. S.; Hitchcock, P. B.; Patel, D.; Smith, J. D.; Zhang, S. *Organometallics* **2000**, *19*, 49.

(11) Eaborn, C.; Ganicz, T.; Hitchcock, P. B.; Smith, J. D.; Sozerli, S. E. *Organometallics* **1997**, *16*, 5621.

10.1021/om800598b CCC: $40.75 © 2008 American Chemical Society
Publication on Web 08/13/2008

Chart 1

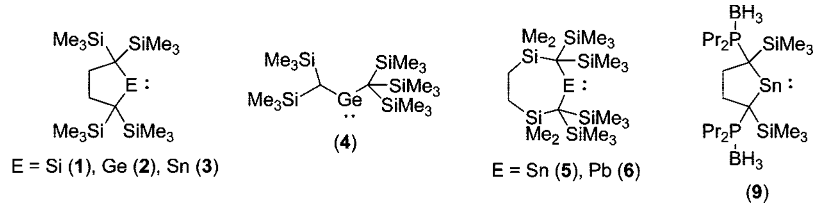

heteroleptic aryl/alkyl-tetrylenes[5d,q,12] and both homoleptic and heteroleptic, intramolecularly base-stabilized diorganotetrylenes have been reported.[13]

Since hydrocarbyl-substituted diorganotetrylenes lack π-donor substituents, they are typically stabilized solely by the use of sterically demanding groups. However, even with very bulky substituents, the heavier dialkyltetrylenes may be subject to dimerization to the corresponding tetraalkylditetrenes $R_2E{=}ER_2$. For example, the archetypal dialkylstannylene $\{(Me_3Si)_2CH\}_2Sn$ (**7**), first reported by Lappert and co-workers in the 1970s, is monomeric in the gas phase, but dimerizes to the distannene $\{(Me_3Si)_2CH\}_2Sn{=}Sn\{CH(SiMe_3)_2\}_2$ in the solid state; in solution **7** is subject to a stannylene−distannene equilibrium.[14] The corresponding dialkylplumbylene $\{(Me_3Si)_2CH\}_2Pb$ (**8**) also forms weakly bonded tetraalkyldiplumbene dimers in the solid state.[1e]

We recently reported a new strategy for the stabilization of dialkyltetrylenes involving agostic-type B−H···E interactions, which alleviate the electron deficiency of the tetrel center in these compounds: the dialkylstannylene $[\{n\text{Pr}_2P(BH_3)\}(Me_3Si)C(CH_2)]_2Sn$ (**9**) crystallizes with either one (*meso*-**9**) or two (*rac*-**9**) short B−H···Sn contacts in the solid state.[15] Spectroscopic and theoretical studies indicate that these short contacts are preserved in solution and are associated with significant delocalization of electron density from the B−H σ-bond into the vacant 5p orbital on tin and so may be classified as genuine B−H···Sn agostic interactions. In order to prove the generality of this strategy for diorganotetrylene stabilization, we have embarked on an extended program to investigate this phenomenon. In this contribution we describe the synthesis of the lead analogue of **9**, $[\{n\text{Pr}_2P(BH_3)\}(Me_3Si)C(CH_2)]_2Pb$ (**10**) (only the second dialkylplumbylene to be structurally characterized), its convenient separation into its two diastereomeric forms, its highly unusual spectroscopic properties, and theoretical studies of the bonding in this compound.

Scheme 1

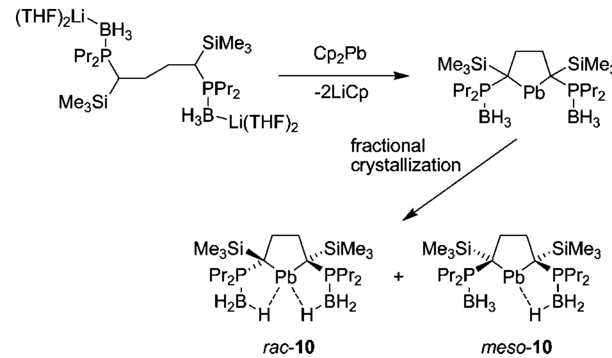

Results and Discussion

Synthesis and Solid State Structures. Whereas the reaction between the dilithium salt $[[\{n\text{Pr}_2P(BH_3)\}(Me_3Si)C(CH_2)]Li(THF)_2]_2$ (**11**) and $SnCl_2$ gives the dialkylstannylene **9** in excellent yield,[15] similar reactions between either $PbCl_2$ or PbI_2 and 1 equiv of **11**, in a variety of solvents and under a variety of conditions, lead to extensive reduction and the deposition of elemental lead; the only hydrocarbon-soluble product from these reactions is the free phosphine-borane $[\{n\text{Pr}_2P(BH_3)\}(Me_3Si)CH(CH_2)]_2$. Such reduction side-reactions may potentially be inhibited through the use of more robust starting materials such as lead amides or aryloxides. However, while reactions between **11** and lead aryloxides such as $Pb(OC_6H_2\text{-}2,6\text{-}t\text{Bu}_2\text{-}4\text{-Me})_2$ yield yellow-orange solutions that have ^{31}P NMR spectra consistent with the formation of **10**, we were unable to separate this compound cleanly from the lithium aryloxide side-products. In contrast, the reaction between Cp_2Pb and 1 equiv of **11** in cold toluene cleanly gives the dialkylplumbylene $[\{n\text{Pr}_2P(BH_3)\}(Me_3Si)C(CH_2)]_2Pb$ (**10**) in excellent yield after a simple workup as a yellow-orange air-sensitive solid (Scheme 1). Crystallization of this solid from cold diethyl ether over 12 h yields the *rac* isomer (*rac*-**10**) exclusively; after removal of all of the *rac* isomer by successive crystallizations from diethyl ether in this way, a clean sample of the *meso* isomer (*meso*-**10**) may be obtained by recrystallization of the residue from cold *n*-hexane. ^{1}H and ^{31}P NMR spectra of the crude product indicate that *rac*- and *meso*-**10** are formed in an approximately 1.5:1 ratio. Compound **10** is sensitive to both heat and light, decomposing to give elemental lead above ca. 80 °C in the solid state or on exposure of a solution in toluene to ambient light at room temperature for several days.

Both *rac*- and *meso*-**10** crystallize as discrete dialkylplumbylene species and represent only the second such species to be crystallographically characterized; the closest Pb···Pb distances in the solid state are in excess of 6.8 Å. The molecular structures of *rac*- and *meso*-**10** are shown in Figure 1, along with selected bond lengths and angles. Both *rac*- and *meso*-**10** crystallize as five-membered metallacycles; for *meso*-**10** there are two crystallographically independent molecules in the asymmetric unit, which differ only trivially in their bond lengths

(12) (a) Eichler, B. E.; Power, P. P. *Inorg. Chem.* **2000**, *39*, 5444. (b) Setaka, W.; Hirai, K.; Sakamoto, K.; Kira, M. *J. Am. Chem. Soc.* **2004**, *126*, 2696. (c) Hino, S.; Olmstead, M.; Phillips, A. D.; Wright, R. J.; Power, P. P. *Inorg. Chem.* **2004**, *43*, 7346.

(13) For examples see:(a) Drost, C.; Hitchcock, P. B.; Lappert, M. F.; Pierssens, L. J.-M. *Chem. Commun.* **1997**, 1141. (b) Drost, C.; Hitchcock, P. B.; Lappert, M. F. *Organometallics* **1998**, *17*, 3838. (c) Wingerter, S.; Gornitzka, H.; Bertermann, R.; Pandey, S. K.; Rocha, J.; Stalke, D. *Organometallics* **2000**, *19*, 3890. (d) Engelhardt, L. M.; Jolly, B. S.; Lappert, M. F.; Raston, C. L.; White, A. H. *J. Chem. Soc., Chem. Commun.* **1988**, 336. (e) Jolly, B. S.; Lappert, M. F.; Engelhardt, L. M.; White, A. H.; Raston, C. L. *J. Chem. Soc., Dalton Trans.* **1993**, 2653. (f) Cardin, C. J.; Cardin, D. J.; Constantine, S. P.; Drew, M. G. B.; Rashid, H.; Convery, M. A.; Fenske, D. *J. Chem. Soc., Dalton Trans.* **1998**, 2749. (g) Benet, S.; Cardin, C. J.; Cardin, D. J.; Constantine, S. P.; Heath, P.; Rashid, H.; Teixeira, S.; Thorpe, J. H.; Todd, A. K. *Organometallics* **1999**, *18*, 389.

(14) (a) Davidson, P. J.; Lappert, M. F. *J. Chem. Soc., Chem. Commun.* **1973**, 317. (b) Goldberg, D. E.; Harris, D. H.; Lappert, M. F.; Thomas, K. M. *J. Chem. Soc., Chem. Commun.* **1976**, 261. (c) Zilm, K. W.; Lawless, G. A.; Merrill, R. M.; Millar, J. M.; Webb, G. G. *J. Am. Chem. Soc.* **1987**, *109*, 7236.

(15) Izod, K.; McFarlane, W.; Tyson, B. V.; Carr, I.; Clegg, W.; Harrington, R. W. *Organometallics* **2006**, *25*, 1135.

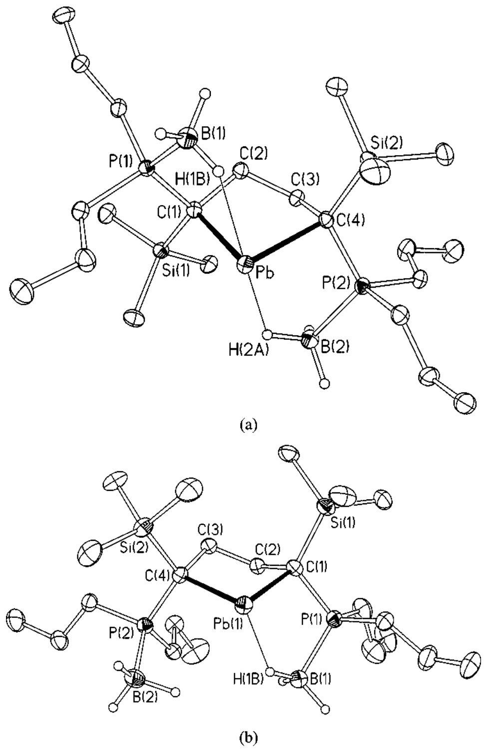

Figure 1. Molecular structures of (a) *rac*-**10** and (b) *meso*-**10** with 40% probability ellipsoids and with H atoms bonded to carbon omitted for clarity. Selected bond lengths (Å) and angles (deg): *rac*-**10**: Pb−C(1) 2.390(4), Pb−C(4) 2.402(4), C(1)−P(1) 1.815(4), C(1)−Si(1) 1.889(4), C(4)−P(2) 1.818(5), C(4)−Si(2) 1.895(4), P(1)−B(1) 1.939(6), P(2)−B(2) 1.945(5), Pb···H(1B) 2.46(6), Pb···H(2A) 2.43(6), C(1)−Pb−C(4) 83.16(15). *meso*-**10** (values for the second molecule in the asymmetric unit in square brackets): Pb(1)−C(1) 2.422(3) [Pb(2)−C(23) 2.372(3)], Pb(1)−C(4) 2.369(3) [Pb(2)−C(26) 2.402(3)], C(1)−P(1) 1.807(3) [C(23)−P(3) 1.810(3)], C(1)−Si(1) 1.885(3) [C(23)−Si(3) 1.895(3)], C(4)−P(2) 1.806(3) [C(26)−P(4) 1.801(3)], C(4)−Si(2) 1.902(3) [C(26)−Si(4) 1.892(3)], P(1)−B(1) 1.932(4) [P(3)−B(3) 1.928(4)], P(2)−B(2) 1.927(4) [P(4)−B(4) 1.941(4)], Pb(1)···H(1B) 2.25(4) [Pb(2)···H(4B) 2.29(4)], C(1)−Pb(1)−C(4) 81.81(10) [C(23)−Pb(2)−C(26) 82.42(10)].

and angles. The Pb−C distances of 2.390(4) and 2.402(4) Å (*rac*-**10**) and 2.369(3) and 2.422(3) Å (*meso*-**10**; 2.372(3) and 2.402(3) Å in the second molecule in the asymmetric unit) are similar to the Pb−C distances in **6** [2.397(6) and 2.411(5) Å];[10] however, the C−Pb−C angles in *rac*- and *meso*-**10** [83.16(15)° and 81.81(10)/82.42(10)°, respectively] are substantially narrower than the corresponding angle in **6** [117.1(2)°] and are slightly narrower than the C−Sn−C angles in *rac*- and *meso*-**9** [85.32(5)° and 84.53(15)°, respectively].[15] The C−Pb−C angles are consistent with (i) the presence of a five-membered metallacycle in *rac*- and *meso*-**10** compared to the seven-membered metallacycle in **6**, (ii) the larger size of the lead atom in **10** versus the tin atom in **9**, and (iii) substantial Pb 6p character in the Pb−C bonds (i.e., substantial 6s character in the lead lone pair). The C−Pb−C angles in **10** are the smallest such angles to be reported to date; typical C−Pb−C angles in acyclic diorganoplumbylenes span the range 91.8(2)° to 121.5(3)°, the narrowest of these C−Pb−C angles being observed in the acyclic heteroleptic diorganoplumbylene $\{2,6\text{-}(C_6H_3\text{-}i\text{-}Pr_2)_2C_6H_3\}PbMe$.[5q]

Perhaps the most striking features of the structures of *rac*- and *meso*-**10** are the short B−H···Pb contacts, two for *rac*-**10** and one for *meso*-**10**; similar short B−H···Sn distances were observed in **9**. In *rac*-**10** the Pb···H(1B) and Pb···H(2A) distances are 2.46(6) and 2.43(6) Å, respectively, whereas in *meso*-**10** the single, short Pb(1)···H(1B) distance is 2.25(4) Å [Pb(2)···H(4B) 2.29(4) Å]; these distances are significantly shorter than the sum of the van der Waals radii of Pb and H (3.22 Å). In addition, *meso*-**10** exhibits a second, somewhat longer Pb···H contact [Pb(1)···H(2C) 2.95(5) Å; Pb(2)···H(3A) 3.04(4) Å in the second molecule in the asymmetric unit], which is, once again, within the sum of the van der Waals radii of Pb and H and which appears to be associated with a much weaker Pb···H interaction (see DFT studies below). For *meso*-**9** no weaker Sn···H interactions were observed, and so we attribute the presence of the second Pb···H interaction in *meso*-**10** to the increased size of the metal atom in this case, which enables the closer approach of a second BH_3 group.

The short, agostic-type B−H···Pb contacts observed in **10** are reminiscent of the agostic-type C−H···Pb contacts proposed for the mixed alkyl/arylplumbylene $(2,4,6\text{-}t\text{Bu}_3C_6H_2)(3,5\text{-}t\text{Bu}_2C_6H_3CMe_2CH_2)Pb$ (**12**),[5d] derived from the spontaneous isomerization of the homoleptic compound $(2,4,6\text{-}t\text{Bu}_3C_6H_2)_2Pb$. However, the Pb···B distances in **10** [3.233 and 3.227 Å (*rac*-**10**); 3.210 Å (for both molecules of *meso*-**10**)] are substantially longer than the Pb···C distances in **12** (2.796 and 2.826 Å), possibly as a consequence of the more rigid nature of the aryl ligand in the latter compound. To the best of our knowledge, the only previous report of a short B−H···Pb contact is in the tris(2-mercaptoimidazolyl)borate complex $(\text{Tm}^{\text{Ph}})_2Pb$ (**13**),[16] in which one of the Tm^{Ph} ligands adopts an inverted η^4-coordination mode, binding the lead atom through its three S-donors and the central B−H group [$\text{Tm}^{\text{Ph}} = HB(2\text{-S},3\text{-PhC}_3N_2)_3$]. In this complex the Pb···H distance is 2.39 Å, similar to the corresponding distances in *rac*- and *meso*-**10**.

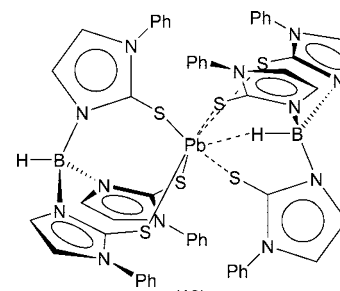

(**13**)

Spectroscopic Characterization. Both *rac*- and *meso*-**10** have been characterized by multielement (^{1}H, ^{13}C{^{1}H}, ^{11}B{^{1}H}, ^{29}Si{^{1}H}, ^{31}P{^{1}H}, and ^{207}Pb{^{1}H}) and variable-temperature NMR spectroscopy. The ^{1}H NMR spectrum of *rac*-**10** in d_8-toluene is largely as expected; the $SiMe_3$ protons give rise to a singlet at 0.29 ppm, while the BH_3 protons give rise to an extremely broad quartet centered at 0.58 ppm, which collapses to a doublet ($J_{PH} = 7.8$ Hz) on selective decoupling of the ^{11}B nucleus, and the diastereotopic propyl groups yield overlapping multiplets in the range 0.88−1.95 ppm. However, somewhat surprisingly, the methylene protons from the backbone of the five-membered metallacycle give rise to multiplets at 2.62 and 6.25 ppm (Figure 2), which collapse to doublets on selective decoupling of the ^{31}P nucleus; this assignment was confirmed by ^{1}H−^{1}H COSY, HSQC, DEPT, and selective ^{1}H{^{31}P} and ^{1}H{^{1}H} experiments. The ^{13}C{^{1}H} spectrum of *rac*-**10** is also largely as expected; the central quaternary carbon atoms of the ligand are observed as a broad doublet at 79.34

(16) Bridgewater, B. M.; Parkin, G. *Inorg. Chem. Commun.* **2000**, *3*, 534.

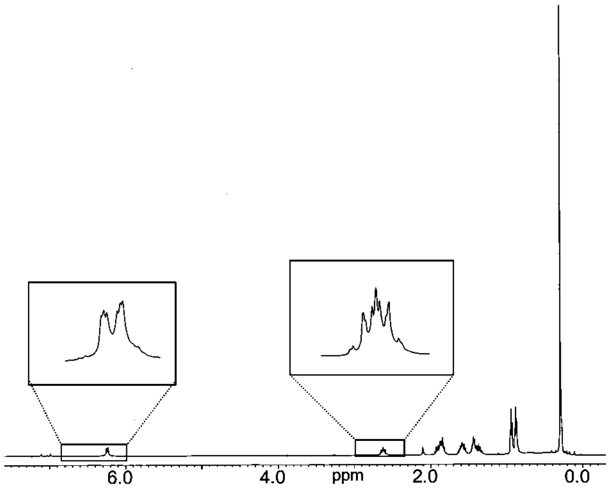

Figure 2. [1]H NMR spectrum of *rac*-**10** in d_8-toluene at room temperature.

ppm (J_{PC} = 4.6 Hz) exhibiting broad satellites due to coupling to ^{207}Pb (J_{PbC} = 660 Hz). The room-temperature ^{31}P{^{1}H} and ^{11}B{^{1}H} spectra of *rac*-**10** consist of a broad quartet and doublet at 23.1 and −43.1 ppm, respectively [J_{PB} = 86 Hz; $\Delta\nu_{1/2}$ (^{31}P) = 240 Hz, $\Delta\nu_{1/2}$ (^{11}B) = 160 Hz].

For *rac*-**10** the ^{1}H, ^{13}C{^{1}H}, ^{11}B{^{1}H}, and ^{31}P{^{1}H} spectra are invariant over the temperature range 20 to −90 °C. In contrast, the variable-temperature ^{1}H, ^{31}P{^{1}H}, and ^{11}B{^{1}H} spectra of *meso*-**10** indicate that this diastereomer is subject to dynamic behavior in solution. At room temperature the ^{1}H NMR spectrum of *meso*-**10** consists of a singlet at 0.13 and a broad quartet at 0.80 ppm, which collapses to a doublet (J_{PH} = 7.8 Hz) on decoupling the ^{11}B nuclei, due to the $SiMe_3$ and BH_3 protons, respectively, a series of overlapping multiplets between 0.88 and 1.95 ppm, due to the diastereotopic propyl groups, and a pair of extremely broad multiplets at 4.54 ppm due to the metallacycle backbone protons. As the temperature is reduced, these signals broaden and decoalesce, until, at −90 °C, the lowest temperature that we were able to attain, the spectrum consists of two singlets at 0.02 and 0.28 ppm, due to the inequivalent $SiMe_3$ groups; a series of overlapping multiplets between 0.85 and 1.83 ppm, due to the BH_3 protons and the propyl groups; and two pairs of broad, poorly resolved multiplets at 2.45 and 2.80 ppm and at 6.59 and 6.76 ppm, due to the backbone methylene protons. The broad quartet observed at 22.9 ppm (J_{PB} = 71 Hz; $\Delta\nu_{1/2}$ = 230 Hz) in the room-temperature ^{31}P{^{1}H} spectrum of *meso*-**10** also broadens and decoalesces as the temperature is reduced, until, at −90 °C, the spectrum consists of two equal intensity, poorly resolved quartets at 18.0 and 24.2 ppm; similarly, the broad doublet observed at −39.0 ppm ($\Delta\nu_{1/2}$ = 170 Hz) in the room-temperature ^{11}B{^{1}H} spectrum of *meso*-**10** also decoalesces at low temperatures such that, at −90 °C, the spectrum consists of two equal intensity, broad, featureless signals at −37.9 and −40.0 ppm. The low-temperature spectra of *meso*-**10** are consistent with the structure obtained in the solid state, in which only one phosphine-borane group is associated with the lead center.

Thus *meso*-**10** exhibits dynamic exchange between the free and bound phosphine-borane groups, which is rapid on the NMR time scale at room temperature (Scheme 2), but which may be frozen out at low temperatures. Similar dynamic behavior was observed for *meso*-**9**; however, whereas *meso*-**9** was subject to a second dynamic process, observed only at very low temperatures, which we attributed to restricted rotation about the P−C bond of the free phosphine-borane group,[15] no such behavior was observed for *meso*-**10**. The lack of a second observable dynamic process for *meso*-**10** may possibly be attributed to the somewhat reduced steric hindrance about the P−C bond in this compound due to the longer Pb−C distance. Line shape analysis of the variable-temperature ^{31}P{^{1}H} spectra of *meso*-**10** yields values of $\Delta H^{\ddagger} = 26 \pm 2$ kJ mol^{-1} and $\Delta S^{\ddagger} = -64 \pm 5$ J K^{-1} mol^{-1} for the phosphine-borane exchange process, consistent with intramolecular exchange.

Scheme 2

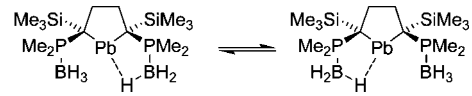

We were unable to distinguish the unique B−H···Pb proton resonances in the ^{1}H{^{11}B} spectra for either diastereomer of **10**, even at −90 °C. This is consistent with rapid exchange among the hydrogen atoms within each BH_3 group on the NMR time scale; a similarly rapid exchange process was observed for the tin analogue **9**.

Perhaps the most striking features of the ^{1}H NMR spectra of *rac*- and *meso*-**10** are the unusual low-field chemical shifts of one set of methylene protons from each metallacycle backbone (Figure 2). Of the two principal conformers of *rac*-**10** it is to be expected that conformer **i** will predominate due to the lack of stabilizing B−H···Pb contacts in conformer **ii** (Chart 2); the ^{1}H, ^{31}P{^{1}H}, and ^{11}B{^{1}H} spectra of *rac*-**10** do not provide any evidence for conformer **ii**. One possible explanation for the unusually large deshielding of one set of backbone protons in **i**, i.e., either H_a or H_b, is their greater exposure to the magnetic effect of diamagnetic circulation of the large, diffuse, essentially 6s-type lone pair on the lead atom. Since H_a is in closer proximity to the lead atom, this would suggest that the signal at 6.25 ppm in *rac*-**10** is due to these protons; however, see below for an alternative explanation.

In contrast to *rac*-**10**, the two principal conformers, **iii** and **iv**, of *meso*-**10** are mirror image forms of equal energy. For this isomer all four backbone protons are inequivalent in any one conformer, but H_a and H_c, and similarly H_b and H_d, may interconvert due to conformational flipping associated with exchange of the free and bound phosphine-borane groups. Therefore, at low temperatures these protons should give rise to four separate signals, with H_a and H_c at similar positions (similarly for H_b and H_d), and these will coalesce at higher temperatures to give two signals at averaged positions, as observed. Once again, due to the proximity of H_a and H_c to the lead(II) center, we tentatively assign the signals at 6.59 and 6.76 ppm in the low-temperature ^{1}H spectrum of *meso*-**10** to these protons.

The ^{207}Pb spectra of *rac*- and *meso*-**10** consist of extremely broad, featureless signals at 4580 ($\Delta\nu_{1/2}$ = 720 Hz) and 5430 ppm ($\Delta\nu_{1/2}$ = 505 Hz), respectively. These values are to substantially higher field than typical chemical shifts for diaryl- or dialkylplumbylenes; for example, the ^{207}Pb chemical shifts of **6**[10] and {2,6-(2,4,6-$Me_3C_6H_2)_2C_6H_3$}$_2$Pb (**14**)[5f] are 10500 and 8844 ppm, respectively. The higher field chemical shift of *rac*-**10** in comparison to that of *meso*-**10** is consistent with the presence of two short, agostic-type interactions in the former, which mitigate the electron deficiency of the lead(II) center, rather than the one such interaction in the latter diastereomer. The chemical shifts observed for **10** are closer to those observed for **12**[5d] and for the fluorine-containing diarylplumbylene {2,4,6-$(CF_3)_3C_6H_2$}$_2$Pb (**15**)[5h] (5067 and 4878 ppm, respectively), in which the electron deficiency of the lead center is mitigated by

Chart 2

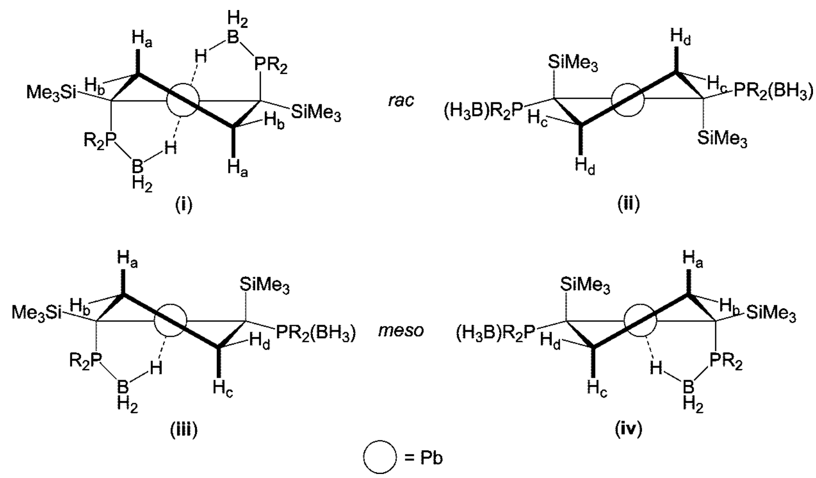

either putative C−H···Pb or C−F···Pb contacts, respectively. The ^{207}Pb chemical shift of *rac*-**10** decreases by 68 ppm at −50 °C, which we attribute to a reduction in the proportion of conformer **ii**. In conformity with this, the ^{207}Pb chemical shift of *meso*-**10** was essentially unchanged over a wide temperature range since the amounts of conformers **iii** and **iv** will be the same at all temperatures.

An inversion−recovery experiment showed that in *rac*-**10** the ^{207}Pb spin−lattice relaxation time, T_1, was 4.1 ms at room temperature. This corresponds to a contribution to line broadening of 78 Hz, so it is clear that the observed line-width of 720 Hz arises mainly from a T_2 mechanism. It has been noted previously that related diorganostannylenes are subject to large ^{119}Sn chemical shift anisotropies (CSA),[17] and this effect will probably be even greater in our lead compounds. However, this mechanism affects T_1 and T_2 to similar extents[18] and so cannot be the major contributor to the latter, although it may dominate T_1. Furthermore, at a reduced measuring field strength (6.9 instead of 11.5 T, corresponding to 0.36 CSA) the ^{207}Pb line-width was essentially unaltered. A contribution to T_2 from modulation of $^3J_{PbB}$ by ^{11}B quadrupolar relaxation would require an unreasonably large value of this coupling to give the observed effect, and the line-widths in the ^{11}B and ^{31}P spectra also show that the ^{11}B relaxation is too slow for this.

An ordinary chemical exchange process can be ruled out on the basis that no corresponding effects are observed in the spectra of any of the other nuclei present in the species. Additionally, the half-height line-widths of the ^{207}Pb spectra of *rac*- and *meso*-**10** increase to 935 and 905 Hz, respectively, at −50 °C, and it is likely that much more profound changes would be observed if chemical exchange were the explanation. We therefore tentatively ascribe the broad nature of these signals to the presence of a low concentration, possibly lead-centered, radical species in rapid equilibrium with the dominant diamagnetic molecules; a similar, although less pronounced, effect was observed in the ^{119}Sn spectra of **9**. This interpretation also provides an alternative explanation for the anomalous shieldings for certain of the backbone protons in *rac*- and *meso*-**10**, namely, that they arise from a pseudocontact interaction with the unpaired electron spin density centered on the lead atom and that the differences between the axial and equatorial protons are due mainly to angular rather than radial dependence.

The solid state infrared spectrum of *rac*-**10** contains bands at 2383, 2181, and 2116 cm^{-1}, which may be attributed to B−H stretching vibrations; the corresponding absorptions for *meso*-**10** occur at 2375 and 2089 cm^{-1}. Comparisons with the vibrational frequencies obtained from DFT calculations (see below) indicate that the red-shifted absorptions at 2181 and 2116 cm^{-1} (*rac*-**10**) and at 2089 cm^{-1} (*meso*-**10**) may be assigned to B−H stretching vibrations for the H atom(s) involved in the B−H···Pb contacts. In solution it is not possible to distinguish the unique B−H(···Pb) stretching vibrations, and only bands at averaged positions are observed.

The UV−visible spectrum of *rac*-**10** contains a principal absorption at 382 nm along with a weaker, broad absorption at approximately 315 nm (ε = 941 and 510 dm^3 mol^{-1} cm^{-1}, respectively), whereas *meso*-**10** exhibits weak to moderate absorptions at 406 and 335 nm (ε = 728 and 1128 dm^3 mol^{-1} cm^{-1}, respectively). These absorptions are independent of solvent polarity (for example, the spectrum of *rac*-**10** in dichloromethane has a principal absorption at 389 nm (ε = 1060 dm^3 mol^{-1} cm^{-1})), excluding charge transfer as their source, and so the lowest energy absorptions may confidently be attributed to a transition between the lone pair and the vacant 6p orbital on the lead atom in each case (see TD-DFT studies below). The higher energy absorptions at 315 and 335 nm for *rac*- and *meso*-**10**, respectively, may be attributed to a transition from the HOMO−1 (C−Pb) orbital to the vacant 6p orbital on the lead atom [σ(C−Pb) → 6p(Pb)]. The yellow color of *rac*- and *meso*-**10** contrasts markedly with the deep red-purple colors of other hydrocarbyl-substituted diorganoplumbylenes. For example, in **6**, the only other crystallographically characterized dialkylplumbylene, the corresponding n → p transition occurs at 610 nm, whereas this transition occurs at 526 nm in the diarylplumbylene **14**. The n → p transition in **10** is much closer to the corresponding transition in **12** (406 nm), and the pale yellow color of **10** is mirrored in the yellow color of **15**; for compounds **12** and **15** either agostic-type C−H···Pb or dative C−F···Pb contacts have been proposed to account for their unusual spectroscopic properties. The blue shift observed for the n → p absorptions in *rac*- and *meso*-**10** may be attributed to perturbation of these orbitals by the B−H···Pb interactions.

DFT Calculations. In order to gain greater insight into the nature of the bonding in **10**, we have undertaken a DFT study of both the *rac* and *meso* diastereomers (*rac*- and *meso*-**10a**, respectively). Although somewhat computationally expensive, calculations were carried out on the complete molecules in order to replicate as completely as possible the B−H···Pb interac-

(17) Eichler, B. E.; Phillips, B. L.; Power, P. P.; Augustine, M. P. *Inorg. Chem.* **2000**, *39*, 5450.

(18) Abragam, A. *The Principles of Nuclear Magnetism*; Oxford University Press: Oxford, UK, 1961; p 316.

Table 1. Comparison of Calculated and Crystallographically Determined Bond Lengths (Å) and Angles (deg) for 10 and 10a

	rac-**10**	*rac*-**10a**	*meso*-**10**[a]	*meso*-**10a**
Pb−C	2.390(4)	2.426	2.422(3)	2.377
	2.402(4)	2.405	2.369(3)	2.462
C−Si	1.889(4)	1.922	1.885(3)	1.929
	1.895(4)	1.922	1.902(3)	1.916
C−P	1.815(4)	1.836	1.807(3)	1.844
	1.818(5)	1.841	1.806(3)	1.828
P−B	1.939(6)	1.957	1.932(4)	1.950
	1.945(5)	1.954	1.927(4)	1.951
B−H(···Pb)	1.01(6)	1.236	1.16(4)	1.248
	1.15(6)	1.240		
B−H[b]	0.94(7)−1.13(5)	1.206−1.208	1.05(5)−1.15(5)	1.205−1.223
H···Pb	2.43(6)	2.385	2.25(4)	2.265
	2.46(6)	2.431		
C−Pb−C	83.16(15)	83.58	81.81(10)	82.24

[a] Values for one of the two crystallographically independent molecules in the asymmetric unit. [b] Range of B−H distances to hydrogen atoms not involved in B−H···Pb interactions.

Table 2. Crystallographic Data for *rac*-10 and *meso*-10

	rac-**10**	*meso*-**10**
formula	$C_{22}H_{56}B_2P_2PbSi_2$	$C_{22}H_{56}B_2P_2PbSi_2$
fw	667.6	667.6
cryst size, mm	0.10 × 0.04 × 0.04	0.34 × 0.30 × 0.20
cryst syst	monoclinic	triclinic
space group	$P2_1/n$	$P\bar{1}$
a, Å	11.4175(8)	11.4623(8)
b, Å	17.6207(13)	14.0466(12)
c, Å	16.6197(12)	22.4174(15)
α, deg		101.861(1)
β, deg	106.796(1)	93.528(1)
γ, deg		114.037(1)
V, Å^3	3201.0(4)	3183.1(4)
Z	4	4
T/K	120	150
ρ_{calcd}, g cm^{-3}	1.385	1.393
μ, mm^{-1}	5.45	5.48
no. reflns measd	33 323	28 521
no. unique reflns, R_{int}	9462, 0.060	14842, 0.022
no. reflns with $F^2 > 2\sigma(F^2)$	8084	12686
trans coeff range	0.612−0.811	0.257−0.407
R, R_w[a] ($F^2 > 2\sigma$)	0.044, 0.090	0.025, 0.058
R, R_w[a] (all data)	0.051, 0.093	0.033, 0.062
S[a]	1.050	1.020
no. of refined params	297	609
max. min. diff map, e Å^{-3}	1.56, −1.43	1.64, −0.79

[a] Conventional $R = \sum||F_o| - |F_c||/\sum|F_o|$; $R_w = [\sum w(F_o^2 - F_c^2)^2/\sum w(F_o^2)^2]^{1/2}$; $S = [\sum w(F_o^2 - F_c^2)^2/(\text{no. data} - \text{no. params})]^{1/2}$ for all data.

tions. Geometry optimizations were performed with the B3LYP hybrid functional[19] with a Lanl2dz effective core potential basis set[20] on the lead atoms and an all-electron 6-31G(d,p) basis set[21] on the remaining atoms; minima were confirmed by the absence of imaginary vibrational frequencies in each case.

The calculated gas-phase structures of *rac*- and *meso*-**10a** closely resemble the structures obtained by X-ray crystallography (Table 1). For both diastereomers the calculated bond lengths are approximately 0.01 to 0.05 Å longer than those determined crystallographically; however, the calculated C−Pb−C angles [83.58° (*rac*-**10a**), 82.24° (*meso*-**10a**)] are very close to those observed in the corresponding crystal structures [83.16(15)° and 81.81(10)/82.42(11)°, respectively].

The short B−H···Pb contacts observed in the crystal structures of *rac*- and *meso*-**10** are reproduced extremely well in the calculated structures; two such contacts are observed for *rac*-**10a** (one from each BH_3 group) and one for *meso*-**10a**. The Pb···H distances for *rac*-**10a** are 2.39 and 2.43 Å, whereas the Pb···H distance in *meso*-**10a** is 2.27 Å; these distances are very similar to those found crystallographically [Pb···H 2.46(6) and 2.43(6) Å (*rac*-**10**); 2.25(4) Å [2.29(4) Å for the second molecule in the asymmetric unit] (*meso*-**10**)]. As expected, the single Pb···H distance in *meso*-**10a** is significantly shorter than the two Pb···H distances in *rac*-**10a**, consistent with weaker B−H···Pb agostic-type interactions in the latter due to competition for the vacant 6p orbital on lead. In addition to the short Pb···H contact in *meso*-**10a**, a somewhat longer contact of 2.828 Å is observed between the lead center and a hydrogen atom in the second BH_3 group; this mirrors the second, longer Pb···H contact observed crystallographically for *meso*-**10** [Pb(1)···H(1B) 2.95(5) Å, Pb(2)···H(3A) 3.04(4) Å]. The *rac* diastereomer is calculated to be 2.8 kcal mol^{-1} more stable than the *meso* diastereomer, consistent with the observation by NMR spectroscopy that *rac*- and *meso*-**10** are formed in an approximately 1.5:1.0 ratio.

Natural bond orbital (NBO) analysis enables an interpretation of the bonding in these molecules based on a set of occupied Lewis-type and unoccupied non-Lewis-type localized orbitals.[22] An NBO analysis of *rac*- and *meso*-**10a** reveals that the HOMO in both diastereomers consists of an essentially pure 6s lone pair [percentage 6s character: 86.7% for both *rac*- and *meso*-**10a**]; the LUMO in each case comprises a pure 6p orbital on the lead atoms which lies orthogonal to the plane of the metallacycle [percentage 6p character: 100% (*rac*-**10a**), 99% (*meso*-**10a**)]. Analysis of the donor−acceptor interactions in **10a** confirms that there is significant delocalization of electron density from the B−H σ-bond(s) into the vacant lead 6p orbital in each case; that is, the short H···Pb contacts are associated with an agostic-type interaction. The $E(2)$ energy, calculated by second-order perturbation theory, provides an estimate of the energies of these interactions; for *rac*-**10a** the $E(2)$ energies for the B−H···Pb interactions are 16.9 and 18.1 kcal mol^{-1}, whereas the $E(2)$ energy for the B−H···Pb interaction in *meso*-**10a** is 24.0 kcal mol^{-1} [the $E(2)$ energy for the second, weaker

(19) (a) Becke, A. D. *J. Chem. Phys.* **1993**, *98*, 5648. (b) Stephens, P. J.; Devlin, F. J.; Chablowski, C. F.; Frisch, M. J. *J. Phys. Chem.* **1994**, *98*, 11623. (c) Hertwig, R. H.; Koch, W. *Chem. Phys. Lett.* **1997**, *268*, 345.

(20) (a) Hay, P. J.; Wadt, W. R. *J. Chem. Phys.* **1985**, *82*, 270. (b) Wadt, W. R.; Hay, P. J. *J. Chem. Phys.* **1985**, *82*, 284. (c) Hay, P. J.; Wadt, W. R. *J. Chem. Phys.* **1985**, *82*, 299.

(21) (a) Hariharan, P. C.; Pople, J. A. *Theor. Chim. Acta* **1973**, *28*, 213. (b) Francl, M. M.; Petro, W. J.; Hehre, W. J.; Binkley, J. S.; Gordon, M. S.; DeFrees, D. J.; Pople, J. A. *J. Chem. Phys.* **1982**, *77*, 3654.

(22) (a) Carpenter, J. E.; Weinhold, F. *J. Mol. Struct. (Theochem)* **1988**, *169*, 41. (b) Carpenter, J. E. Ph.D. Thesis, University of Wisconsin, Madison, WI, 1987. (c) Foster, J. P.; Weinhold, F. *J. Am. Chem. Soc.* **1980**, *102*, 7211. (d) Reed, A. E.; Weinhold, F. *J. Chem. Phys.* **1983**, *78*, 4066. (e) Reed, A. E.; Weinhold, F. *J. Chem. Phys.* **1983**, 1736. (f) Reed, A. E.; Weinstock, R. B.; Weinhold, F. *J. Chem. Phys.* **1985**, *83*, 735. (g) Reed, A. E.; Curtiss, L. A.; Weinhold, F. *Chem. Rev.* **1988**, *88*, 899.

B−H···Pb interaction is just 3.4 kcal mol^{-1}]. Selective deletion of the principal agostic-type interactions (using the NBODel routine in NBO 3.0)[23] suggests that these interactions afford an overall stabilization energy of approximately 40.6 (for the two B−H···Pb contacts) and 26.5 kcal mol^{-1} for *rac*- and *meso*-**10a**, respectively. For *meso*-**10a** deletion of both the principal and the weaker, secondary B−H···Pb interactions suggests a combined stabilization energy of 30.3 kcal mol^{-1} for this diastereomer. As expected, the B−H···Pb interactions in **10a** are somewhat less stabilizing than the corresponding B−H···Sn interactions in **9**, consistent with the larger, more diffuse 6p orbitals on the lead center; using the above methodology, we calculate that the corresponding stabilization energies associated with the B−H···Sn agostic interactions in *rac*- and *meso*-**9** are 45.1 (for the two B−H···Sn contacts) and 33.8 kcal mol^{-1}, respectively.

Frequency calculations reveal that the B−H stretching vibrations in **10a** occur in the ranges 2168−2449 cm^{-1} (*rac*-**10a**) and 2128−2468 cm^{-1} (*meso*-**10a**), after scaling[24] [cf. 2116−2383 and 2089−2374 cm^{-1} for the observed B−H stretching vibrations in *rac*- and *meso*-**10**, respectively]. The B−H stretching vibrations associated with the B−H···Pb interactions are clearly identified as those occurring at 2168 and 2221 cm^{-1} (*rac*-**10a**; cf. 2116 and 2181 cm^{-1} observed in *rac*-**10**) and 2128 cm^{-1} (*meso*-**10a**; cf. 2089 observed in *meso*-**10**). The calculations predict a red shift for these absorptions compared to the remaining B−H stretching vibrations of between 188 and 281 cm^{-1} for *rac*-**10a** and between 173 and 340 cm^{-1} for *meso*-**10a**; these compare well with the observed red shifts of between 202 and 267 cm^{-1} for *rac*-**10** and of 285 cm^{-1} for *meso*-**10**.

TD-DFT calculations were performed on *rac*- and *meso*-**10a**, both in the gas phase and with solvation by heptane (using the EIF-PCM model as implemented in Gaussian03).[25] Little difference was observed between these two sets of calculations, and so the following discussion relates only to the results that explicitly include solvation. The calculations reveal that the lowest energy absorptions observed in the UV−visible spectra of *rac*- and *meso*-**10** are associated with n → p transitions at the lead center in each case. The lowest energy transitions to singlet excited states are calculated to occur at 333 and 366 nm for *rac*- and *meso*-**10a**, respectively. However, for both *rac*- and *meso*-**10a**, there is a low-lying triplet state just 12.5 (*rac*-**10a**) and 11.5 kcal (*meso*-**10a**) above the ground state.

The low-lying triplet states of *rac*- and *meso*-**10** can be observed experimentally. Irradiation of frozen solutions of *rac*-**10** in methylcyclohexane at either of the absorption maxima (315 or 382 nm) yields essentially identical phosphorescence spectra consisting of two distinct maxima at 462 and 523 nm ($\tau = 9.7\ \mu$s); similarly, irradiation of *meso*-**10** at either 335 or 406 nm yields essentially identical phosphorescence spectra with two distinct maxima at 454 and 528 nm ($\tau = 9.9\ \mu$s). Phosphorescence from s^2 heavy metal centers such as Pb(II) has been observed previously and has been assigned to the $^3P_1 \rightarrow {}^1S_0$ transition, consistent with our observations.[26]

Attempts to calculate the ^{1}H NMR spectra of **10** using the GIAO method[27] were unsuccessful. While the chemical shifts of the $SiMe_3$ and propyl protons were satisfactorily modeled, the chemical shifts of the backbone protons were calculated to lie between 1.91 and 2.24 ppm for *rac*-**10a** and between 0.65 and 2.14 ppm for *meso*-**10a**. Clearly, these results are not in agreement with the highly unusual chemical shifts observed experimentally for the methylene backbone protons, although this may be an artifact of the ECP basis set used for the lead atoms in these calculations.

Conclusions

Although the synthesis of dialkylplumbylenes is often hampered by reduction of lead(II) starting materials such as $PbCl_2$ or PbI_2 to give elemental lead, we find that use of the more robust precursor Cp_2Pb enables the synthesis of a novel cyclic dialkylplumbylene (**10**). This compound may readily be separated into its constituent diastereomers via a straightforward fractional crystallization process, and both diastereomers have been characterized by X-ray crystallography; this represents only the second structural characterization of a dialkylplumbylene. The solid state structures of *rac*- and *meso*-**10** reveal that the lead(II) center forms part of a five-membered plumbacycle in each case and that there are either one (*meso*-**10**) or two (*rac*-**10**) short, agostic-type Pb···H contacts; in addition, the large Pb center enables a second, weaker Pb···H contact in *meso*-**10** that is not observed in its tin(II) analogue. The agostic nature of these contacts is evident from the infrared, UV−visible, and multielement NMR spectra of both *rac*- and *meso*-**10**. DFT studies also confirm that there is substantial delocalization of B−H σ-bonding electron density into the vacant 6p orbital of the lead center in each diastereomer. This delocalization stabilizes *rac*- and *meso*-**10** by 40.6 and 30.3 kcal mol^{-1}, respectively. Thus, it appears that such agostic-type interactions may provide a new, general method for the stabilization of diorganotetrylenes.

Experimental Section

All manipulations were carried out using standard Schlenk techniques under an atmosphere of dry nitrogen or argon. Diethyl ether, *n*-hexane, methylcyclohexane, and toluene were distilled under nitrogen from sodium/potassium alloy, whereas dichloromethane was distilled from CaH_2 under nitrogen; all solvents were stored over a potassium film, except dichloromethane, which was stored over activated 4 Å molecular sieves. Deuterated toluene was distilled from potassium, deoxygenated by three freeze−pump−thaw cycles, and stored over activated 4 Å molecular sieves. All compounds were used as supplied by the manufacturer, except [[{nPr$_2$P(BH$_3$)}(Me$_3$Si)C(CH$_2$)]Li(THF)$_2$]$_2$ (**11**),[28] which was prepared by a previously published method, and Cp_2Pb, which was prepared by a modification of a literature method (see below).[29]

NMR spectra were recorded on a JEOL Lambda500 spectrometer operating at 500.16 (^{1}H), 125.65 (^{13}C), 160.47 (^{11}B), 99.37 (^{29}Si), 202.47 (^{31}P), and 104.32 (^{207}Pb) MHz, respectively; chemical shifts are quoted in ppm relative to tetramethylsilane (^{1}H, ^{13}C, and ^{29}Si),

(23) Wong, M. W. *Chem. Phys. Lett.* **1996**, *256*, 391.
(24) NIST Computational Chemistry Comparison and Benchmark Database, NIST Standard Reference Database Number 101, Release 14, Sept 2006, Editor: Russell D. Johnson III, http://srdata.nist.gov/cccbdb.
(25) (a) Cancès, M. T.; Mennucci, B.; Tomasi, J. *J. Chem. Phys.* **1997**, *107*, 3032. (b) Mennucci, B.; Tomasi, J. *J. Chem. Phys.* **1997**, *106*, 5151. (c) Mennucci, B.; Cancès, E.; Tomasi, J. *J. Phys. Chem. B* **1997**, *101*, 10506. (d) Tomasi, J.; Mennucci, B.; Cancès, E. *J. Mol. Struct. (THEOCHEM)* **1999**, *464*, 211.
(26) Nikol, H.; Becht, A.; Vogler, A. *Inorg. Chem.* **1992**, *31*, 3277.
(27) (a) McWeeny, R. *Phys. Rev.* **1962**, *126*, 1028. (b) Ditchfield, R. *Mol. Phys.* **1974**, *27*, 789. (c) Dodds, J. L.; McWeeny, R.; Sadlej, A. J. *Mol. Phys.* **1980**, *41*, 1419. (d) Wolinski, K.; Hilton, J. F.; Pulay, P. *J. Am. Chem. Soc.* **1990**, *112*, 8251.
(28) Izod, K.; McFarlane, W.; Tyson, B. V.; Clegg, W.; Harrington, R. W. *Chem. Commun.* **2004**, 570.
(29) (a) Fischer, E. O.; Grubert, H. *Z. Anorg. Allg. Chem.* **1956**, *286*, 237. (b) Armstrong, D. R.; Davidson, M. G.; Moncrieff, D.; Russell, C. A.; Stourton, C.; Steiner, A.; Stalke, D.; Wright, D. S. *Organometallics* **1997**, *16*, 3340.

external $BF_3(OEt_2)$ (^{11}B), external 85% H_3PO_4 (^{31}P), and external Me_4Pb (^{207}Pb), as appropriate. The positions of the BH_3 signals in the ^{1}H NMR spectra of *rac*- and *meso*-**10** and J_{PH} for these signals were determined using a selective ^{1}H{^{11}B} experiment; spectral assignments in the ^{1}H and ^{13}C{^{1}H} spectra were aided by the use of ^{1}H−^{1}H COSY, HSQC, DEPT, and selective ^{1}H{^{1}H} and ^{1}H{^{31}P} experiments. The spin−lattice relaxation time in *rac*-**10** was determined by a standard inversion recovery experiment. UV−visible spectra were recorded in matched quartz cells as 1.0 mM solutions in methylcyclohexane or dichloromethane on a Hitachi U-3010 spectrometer; low-temperature phosphorescence spectra were recorded using optically dilute solutions in methylcyclohexane on a Hitachi F-4500 spectrophotometer; phosphorescence lifetimes were measured on a PTI Easy Life spectrometer using the Xeno flash system and fitted using the included software. Infrared spectra were recorded either as powders or as solutions in methylcyclohexane on a Nicolet Avatar 370DTGS spectrometer. Elemental analyses were obtained by the Elemental Analysis Service of London Metropolitan University.

Preparation of Cp_2Pb. This is a modification of the procedure previously reported by Fischer and Grubert.[29] To a slurry of PbI_2 (14.10 g, 30.6 mmol) in THF (20 mL) was added a solution of CpNa (5.39 g, 61.2 mmol) in THF (20 mL). This solution was stirred for 1 h and solvent was removed *in vacuo*. Pure Cp_2Pb was obtained by sublimation of the solid residue at 150 °C/10^{-7} mmHg. Yield: 3.92 g, 38%. [N.B. the previously reported difficulty in dealing with the sublimation residue, where spontaneous ignition has been observed, is avoided by the use of PbI_2 as a starting material.]

Preparation of [{nPr$_2$P(BH$_3$)}(Me$_3$Si)C(CH$_2$)]$_2$Pb (10). To a cold (−78 °C) solution of freshly sublimed Cp_2Pb (0.51 g, 1.52 mmol) in toluene (20 mL) was added, dropwise, a cold (−78 °C) solution of [{nPr$_2$P(BH$_3$)}(Me$_3$Si)C(CH$_2$)]$_2$Li$_2$(THF)$_4$ (1.16 g, 1.52 mmol) in toluene (20 mL), excluding light as much as possible. This mixture was allowed to attain room temperature and was stirred for 18 h. Solvent was removed *in vacuo*, and the product was extracted into diethyl ether (3 × 15 mL) and filtered. The yellow solution was concentrated to 10 mL and cooled to −30 °C for 1 week. The yellow plates of *rac*-**10** that had deposited after this time were isolated by filtration; this process was repeated twice more to give two more batches of *rac*-**10** (combined yield 0.49 g). After this process the solvent was removed *in vacuo* from the filtrate, and the orange oil was dissolved in *n*-hexane (10 mL) and cooled to −30 °C for 24 h. The orange blocks of *meso*-**10** that deposited were isolated by filtration (yield 0.40 g). Combined yield of *rac*- and *meso*-**10**: 0.89 g, 88%. Anal. Calcd for $C_{22}H_{56}B_2P_2PbSi_2$: C, 39.58; H 8.45. Found: C, 39.72; H 8.32. Mp: 88 °C [dec (*rac*-**10**)], 81 °C [dec (*meso*-**10**)].

Spectroscopic Data for *rac*-10. ^{1}H{^{11}B} NMR (d_8-toluene, 20 °C): δ 0.29 (s, 18H, SiMe$_3$), 0.58 (d, J_{PH} = 7.8 Hz, 6H, BH$_3$), 0.88 (t, $^3J_{HH}$ = 6.9 Hz, 6H, CH$_2$CH$_2$*CH$_3$*), 0.94 (t, $^3J_{HH}$ = 6.7 Hz, 6H, CH$_2$CH$_2$*CH$_3$*), 1.33−1.95 (m, 16H, *CH$_2$CH$_2$*CH$_3$), 2.62 (m, 2H, CH$_2$CH$_2$), 6.25 (m, 2H, CH$_2$CH$_2$). ^{13}C{^{1}H} NMR (d_8-toluene, 20 °C): δ 3.73 (d, J_{PC} = 1.9 Hz, SiMe$_3$), 16.04 (d, J_{PC} = 14.4 Hz, 2 x CH$_2$CH$_3$), 16.78 (*CH$_2$CH$_2$*CH$_3$), 18.40 (*CH$_2$CH$_2$*CH$_3$), 30.72 (d, J_{PC} = 39.3 Hz, *CH$_2$CH$_2$*CH$_3$), 36.06 (d, J_{PC} = 22.1 Hz, *CH$_2$CH$_2$*CH$_3$), 41.16 (d, J_{PC} = 18.2 Hz, CH$_2$CH$_2$), 79.34 (d, J_{PC} = 4.6 Hz, J_{PbC} = 660 Hz, CPb). ^{11}B{^{1}H} (d_8-toluene, 20 °C): δ −43.1 (br d, J_{PB} = 86 Hz). ^{29}Si (d_8-toluene, 20 °C): δ 0.57 (d, J_{SiP} = 8.5 Hz). ^{31}P{^{1}H} (d_8-toluene, 20 °C): δ 23.1 (br q, J_{PB} = 86 Hz). ^{207}Pb{^{1}H} (d_8-toluene, 20 °C): δ 4580 (br s). UV/vis (1.0 mM in methylcyclohexane): λ_{max} 382 nm (ε = 941 dm^3 mol^{-1} cm^{-1}), 315 nm (ε = 510 dm^3 mol^{-1} cm^{-1}). IR (cm^{-1}): 2962 (m), 2931 (m), 2871 (m), 2826 (m), 2810 (m), 2383 (m), 2189 (m), 2116 (m), 1461 (m), 1454 (m), 1246 (s), 1076 (m), 1048 (m), 1034 (m), 978 (m), 902 (m), 883 (s), 847 (s), 831 (s), 772 (m), 755 (s), 712 (m), 685 (m), 675 (m), 643 (s), 602 (m), 581 (s), 456 (m), 434 (s), 421 (m), 410 (m), 408 (m).

Spectroscopic Data for *meso*-10. ^{1}H{^{11}B} NMR (d_8-toluene, 20 °C): δ 0.13 (s, 18H, SiMe$_3$), 0.80 (d, J_{PH} = 9.2 Hz, 6H, BH$_3$), 0.94 (t, $^3J_{HH}$ = 6.9 Hz, 6H, CH$_2$CH$_2$*CH$_3$*), 0.96 (t of d, $^3J_{HH}$ = 6.7 Hz, $^4J_{PH}$ = 0.9 Hz, CH$_2$CH$_2$*CH$_3$*), 1.30−1.97 (m, 16H, *CH$_2$CH$_2$*CH$_3$), 4.40 (br m, 2H, CH$_2$CH$_2$), 4.67 (br m, 2H, CH$_2$CH$_2$). ^{13}C{^{1}H} NMR (d_8-toluene, 20 °C): δ 2.01 (SiMe$_3$), 16.09 (d, J_{PC} = 13.4 Hz, CH$_2$*CH$_3$*), 16.24 (d, J_{PC} = 13.4 Hz, CH$_2$*CH$_3$*), 16.77 (*C*H$_2$CH$_3$), 18.10 (d, J_{PC} = 1.9 Hz, *C*H$_2$CH$_3$), 32.08 (d, J_{PC} = 27.8 Hz, *CH$_2$*CH$_2$CH$_3$), 33.77 (d, J_{PC} = 31.7 Hz, *CH$_2$*CH$_2$CH$_3$), 42.85 (d, J_{PC} = 7.7 Hz, CH$_2$CH$_2$), 89.84 (br, CPb). ^{11}B{^{1}H} (d_8-toluene, 20 °C): δ −39.0 (br d, J_{PB} = 71 Hz). ^{29}Si NMR (d_8-toluene, 20 °C): δ −2.80 (d, J_{SiP} = 2.42 Hz). ^{31}P{^{1}H} NMR (d_8-toluene, 20 °C): δ 22.9 (br q, J_{PB} = 71 Hz). ^{207}Pb{^{1}H} NMR (d_8-toluene, 20 °C): δ 5430 (br s). UV/vis (1.0 mM in methylcyclohexane): λ_{max} 406 nm (ε = 728 dm^3 mol^{-1} cm^{-1}), 335 nm (ε = 1128 dm^3 mol^{-1} cm^{-1}). IR (cm^{-1}): 2959 (m), 2931 (m), 2896 (m), 2871 (m), 2375 (m), 2299 (w), 2089 (m), 1462 (m), 1454 (m), 1403 (s), 1376 (w), 1337 (w), 1245 (s), 1228 (m), 1127 (w), 1075 (m), 1065 (m), 1039 (m), 1021 (m), 984 (m), 909 (m), 889 (m), 834 (s), 802 (s), 741 (m), 684 (m), 676 (m), 652 (m), 636 (m), 618 (m), 581 (m), 455 (m), 444 (m), 431 (m).

Crystal Structure Determinations of *rac*- and *meso*-10. Measurements were made on Bruker APEX2 and SMART 1K CCD diffractometers using synchrotron radiation (λ = 0.6895 Å) for *rac*-**10** and graphite-monochromated Mo Kα radiation (λ = 0.71073 Å) for *meso*-**10**. For both compounds cell parameters were refined from the observed positions of all strong reflections in each data set. Intensities were corrected semiempirically for absorption, based on symmetry-equivalent and repeated reflections, and for incident beam decay for *rac*-**10**. The structures were solved by direct methods and refined on F^2 values for all unique data. Table 2 gives further details. The hydrogen atoms of the BH_3 groups were located in difference maps and were freely refined. Non-hydrogen atoms were refined anisotropically, and all remaining H atoms were constrained with a riding model; U(H) was set at 1.2 (1.5 for methyl groups) times U_{eq} for the parent atom. Minor disorder was resolved for one propyl group in the second molecule of *meso*-**10**. Programs were Bruker AXS APEX2, SMART (control) and SAINT (integration), and SHELXTL for structure solution, refinement, and molecular graphics.[30]

DFT Calculations. Geometry optimizations on the gas-phase molecules were performed with the Gaussian03 suite of programs (revision C.02)[31] on a 224-core Silicon Graphics Altix 4700 computer with 1.6 GHz Montecito Itanium2 processors and 896 Gb of memory, via the EPSRC National Service for Computational Chemistry Software (http://www.nsccs.ac.uk). Optimizations were performed using the B3LYP hybrid functional[19] with a Lanl2dz effective core potential basis set[20] for Pb and a 6-31G(d,p) all-electron basis set on the remaining atoms[21] [default parameters were used throughout]. Minima were confirmed by the absence of imaginary vibrational frequencies; vibrational frequencies were corrected using a scaling factor of 0.961.[24] Natural bond orbital analyses were performed using the NBO 3.0 module of Gaussian03;[22] the stabilization energy associated with the B−H···Pb interactions was calculated using the NBODel routine in which the elements affording this interaction were selectively deleted.[23] NMR shielding tensors were calculated using the GIAO method at the B3LYP/Lanl2dz,6-311++G(2d,p)//Lanl2dz,6-31G(d,p) level of theory; chemical shifts are quoted in ppm relative to TMS calculated

(30) (a) *APEX2*, *SMART*, and *SAINT* software for CCD diffractometers; Bruker AXS Inc.: Madison, WI, 2004 and 1997. (b) Sheldrick, G. M. *Acta Crystallogr., Sect. A* **2008**, *64*, 112.

(31) Frisch, M. J.; et al. *Gaussian 03*, Revision C.02; Gaussian, Inc.: Wallingford, CT, 2004.

at the same level of theory.[27] TD-DFT studies were carried out at the B3LYP/Lanl2dz,6-31G(d,p) level of theory, both in the gas phase and with solvation by heptane, the latter using the EIF-polarizable continuum model implemented in Gaussian03.[25]

Acknowledgment. The authors are grateful to the EPSRC for financial support and to the EPSRC-funded National Crystallography Service and STFC for access to synchrotron facilities; Mr. K. Elliott and Prof. A. Harriman are thanked for the phosphorescence measurements on *rac*- and *meso*-**10**.

Supporting Information Available: For *rac*- and *meso*-**10** details of structure determination, atomic coordinates, bond lengths and angles, and displacement parameters in CIF format. For *rac*- and *meso*-**10a** details of DFT calculations, final atomic coordinates, and energies. Complete details of ref 31. This material is available free of charge via the Internet at http://pubs.acs.org. Observed and calculated structure factor details are available from the authors upon request.

OM800598B